PRELIMINARY RESULT OF POLARIZATION PROPERTY ANALYSIS USING FULLY POLARIMETRIC GB-SAR IMAGES

Moon-Kyung Kang[1], Kwang-Eun Kim[1], Hoonyol Lee[2], Seong-Jun Cho[1], and Jae-Hee Lee[1]

[1] Mineral Resources Research Division, Korea Institute of Geoscience and Mineral Resources, Daejeon, Republic of Korea (kangmk@kigam.re.kr, kimke@kigam.re.kr, mac@kigam.re.kr, zack@kigam.re.kr)

[2] Department of Geophysics, Kangwon National University, Chuncheon, Republic of Korea (hoonyol@knu.ac.kr)

ABSTRACT

The Korea Institute of Geoscience and Mineral Resources (KIGAM) and Kangwon National University (KNU) GB-SAR team have been developed a fully polarimetric and interferometric GB-SAR system over past several years. The main objective of this study is to analyse a polarimetric characteristics of various terrain targets measured by a polarimetric GB-SAR system and to confirm a compatible and effective polarimetric analysis method to reveal the polarization properties of different terrain targets. We focused on an application of this polarimetric GB-SAR image and a basic analysis method to extract a polarization property from different terrain targets as a preliminary study. An unsupervised classification method were applied for analysis of a fully polarimetric GB-SAR image, in particular, a combined H/A/$\underline{\alpha}$ and the complex Wisahrt classifier method [1] based on the H/A/$\underline{\alpha}$ polarimetric decomposition theorem [2], [3].

The simplified schematic configuration of the GB-SAR system is shown in Fig. 1 [4], and measurement specifications are listed in Table 1. The GB-SAR system consists of two instrument parts which are a radio frequency (RF) system part based on a Vector Network Analyzer (VNA) and a motion controlling part. The RF instrumentation composed of a VNA, a power amplifier, and a dual polarization square horn antenna. And a PXI (PCI eXtensions for Instrumentation) or a notebook computer controls a VNA, a motion of the antennas, and data recording. This GB-SAR system has a capability of measuring a fully polarimetric and interferometric SAR data and multi-frequency data, at C-band (5.3 ㎓) and X-band (9.65 ㎓) and its flexibility of a measurement for various natural and artificial targets. The C-band fully polarimetric SAR data used in this study was obtained at 160 times during 3 days between 3rd and 5th November, 2008 in late autumn season of Korea. The outdoor test site was located inside KIGAM field and the radar measurement position where located on 4th floor building height. There are a little rise heap area covered with trees and grass, around flat grass field, and several artificial targets such as wooden geomagnetic observation boxes and metallic poles and panels in the test site. Five metallic trihedral corner reflector (side length: 50 ㎝) was used to obtain a high radar cross section (RCS) reference.

In this study, we used the 'gbsar' processor developed by KNU for a GB-SAR focusing processing. Lee *et al*. [4], [5] already described that the characteristics, advantage, and limitations according to different SAR focusing algorithm such as Deramp-FFT (DF) and Range-Doppler (RD) algorithm. After a SAR focusing processing, we used an open software package, named 'PolSARpro' for a polarimetric analysis and classification of the polarimetric GB-SAR image. The observed polarimetric GB-SAR data was processed by the Deramp-FFT (DF) algorithm for a SAR focusing processing. And a multi-looking and the Lee refined SAR speckle filtering [3] were applied for speckle reduction and data compression. And then a multi-looking image was processed by an H/A/$\underline{\alpha}$ polarimetric classification method and H/$\underline{\alpha}$ or H/A/$\underline{\alpha}$ unsupervised classification combined with the Wishart classifier algorithm before and after the speckle filtering processing.

Fig. 2 shows a Sinclair color-coded image of VV, HV and HH components as red, green, and blue colors respectively. Five permanent scatterers were represented white and pink-magenta color associated with a strong backscattering property, also appeared at man-made targets such as several geomagnetic measurement boxes and metallic poles. Over the grass area, the green color indicates a dominant HV component, generally characteristics of vegetated field. Fig. 3 shows the segmentation images and distribution results in H/$\underline{\alpha}$, H/A, and A/$\underline{\alpha}$ planes based on Cloude and Pottier's method. The H/A/$\underline{\alpha}$ polarimetric classification and distribution result in H/$\underline{\alpha}$ plane were separated a pixel element of the GB-SAR image into zone 8 and zone 5 dominantly. The zone 8 and 5 characterize low entropy dipole scattering and medium entropy vegetation scattering respectively. The trees and a part of grass area were classified zone 5 and the whole grass area was segmented on zone 8. Zone 5 would include scattering from vegetated surfaces with anisotropic scatterers and moderated correlation of scatterer orientations. An isolated dipole scatterer would appear in the 8 zone, as would scattering from vegetation with strongly correlated orientation of anisotropic scattering elements. 5 permanent scatterers appeared red color pixels in the H/$\underline{\alpha}$ classification image distributed in zone 7.

The unsupervised classification method based on the H/A/$\underline{\alpha}$ decomposition and the complex Wishart classifer algorithm were used to extract the classification information of different terrain types for the GB-SAR image. We thought that the classification results after the Lee refined speckle filter show better result than ones before the speckle filtering. The man-made targets such as 5 corner reflectors, wood boxes, and metallic poles were separated from a natural media such as trees area after multi-looking and the Lee refined filtering. Fig. 4 shows the Wisahrt-H/α classification image and enlarged images at several example points that represent 5 corner reflectors, 2 man-made targets, and 4 trees positions and the corresponding values were listed in the below table. The HH, HV, VH, and VV values are extracted from an amplitude image and T11, T22, T33, and span values computed from T3 coherency matrix. The position for 5 permanent scatterers is represented ps_1, as ps_2, ps_3, ps_4, and ps_5. The md_1 and md_2 are the point for 2 artificial targets and tr_1, tr_2, tr_3, and tr_4 are related to a tree area. We can see that the 5 permanent scatterers and 2 man-made targets were classified to same class 4. The tr_2 position classified in class 4 that may be a role like as a corner reflector and the other trees area divided

to class 6. As shown in some cases, these targets were not distinguished only by a numerical difference between a natural media and an artificial target. For example, the ps_2 and tr_3 are similar in value but these areas are separated in a different class, class 4 and class 6. And the md_2 and tr_4 also are classified a different class even though they has a few numerical difference.

The polarimetric characteristics of various terrain targets contained in the fully polarimetric GB-SAR data were discussed to confirm a compatible and effective polarimetric analysis method to reveal a polarization property of different terrain targets. The result show that an unsupervised classification method based on H/A/$\underline{\alpha}$ polarimetric decomposition method can be effective and useful to discriminate between a natural and an artificial target. And the developed GB-SAR system could be used as a convenient tool for the analysis of polarimetric properties for various terrain targets.

ACKNOWLEDGEMENTS

This research was supported by a grant (07KLSGC03) from Cutting-edge Urban Development – Korean Land Spatialization Research Project funded by Ministry of Land, Transport and Maritime Affairs of Korean government.

REFERENCES

[1] J. -S. Lee, M. R. Grunes, T. L. Ainsworth, L. -J. Du, D. L. Schuler, and S. R. Cloude, "Unsupervised Classification Using Polarimetric Decomposition and the Complex Wishart Classifier," *IEEE Transactions on Geoscience and Remote Sensing*, vol. 37, no. 5, pp. 2249-2258, 1999.

[2] S. R. Cloude and E. Pottier, "An Entropy Based Classification Scheme for Land Applications of Polarimetric SAR," *IEEE Transactions on Geosciences and Remote Sensing*, vol. 35, no. 1, pp. 68-78, 1997.

[3] J. -S. Lee and E. Pottier, *Polarimetric Radar Imaging from Basics to Applications*, CRC Press, Boca Raton, FL, USA, 2009.

[4] H. Lee, S. -J. Cho, N. -H. Sung, and J. -H. Kim, "Development of a GB-SAR (I): System Configuration and Interferometry," *Korean Journal of Remote Sensing*, vol. 23, no. 4, pp. 237-245, 2007a.

[5] H. Lee, S. -J. Cho, N. -H. Sung, and J. -H. Kim, "Development of a GB-SAR (II): Focusing Algorithms," *Korean Journal of Remote Sensing*, vol. 23, no. 4, pp. 247-256, 2007b.

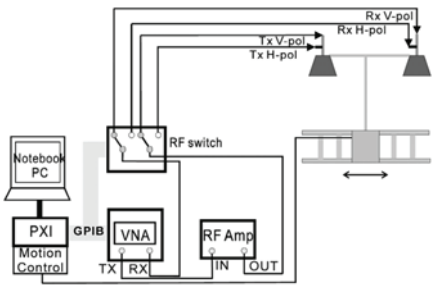

Fig. 1. Configuration of a GB-SAR system.

Table 1 GB-SAR system measurement characteristics.

center frequency	5.3 GHz
range bandwidth	600 MHz
IF bandwidth	1 kHz
number of point	1601
power	calibration: VNA -40 dBm, Amp 33 dBm acquisition: VNA 0 dBm, Amp 33 dBm
azimuth sampling step	5 cm
azimuth length	5 m
polarization mode	quad-polarization (HH, HV, VH, and VV)
maximum range	~ 200 m

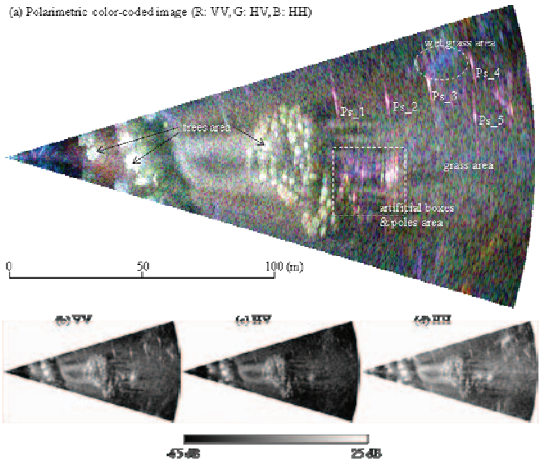

Fig. 2. An example of three polarimetric component amplitude images in dB and the corresponding polarimetric color-coded image.

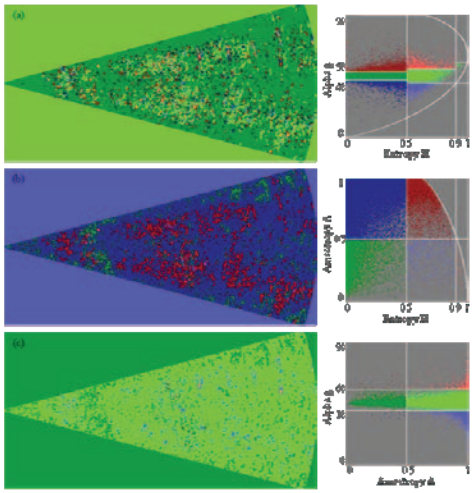

Fig. 3. An example of the H/A/$\bar{\alpha}$ polarimetric classification results in (a) H/$\bar{\alpha}$, (b) H/A, and (c) A/$\bar{\alpha}$ plane using the Cloude and Pottier's method applied with 3 window size before the Lee refined speckle filtering.

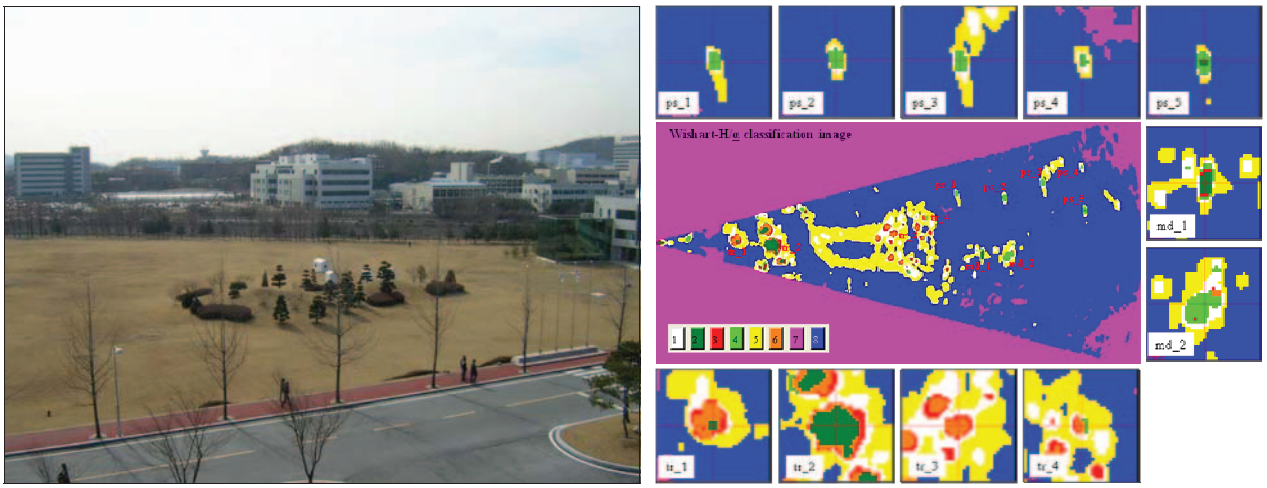

Value (dB)	ps_1	ps_2	ps_3	ps_4	ps_5	md_1	md_2	tr_1	tr_2	tr_3	tr_4
HH	9.670	11.936	7.834	2.902	15.201	26.061	4.090	16.681	23.446	11.427	4.644
HV	-20.418	-16.495	-11.788	-19.386	-12.957	-15.144	-12.335	7.674	-7.521	-2.212	-10.753
VH	-21.840	-20.111	-14.021	-22.385	-17.274	-11.312	-15.288	5.486	1.691	-5.333	-12.309
VV	7.617	11.539	8.879	1.315	12.561	14.960	10.612	9.292	13.498	-0.242	6.175
T11	20.489	26.398	3.665	7.366	31.108	49.455	18.794	31.665	43.246	20.392	13.881
T22	8.682	10.274	19.742	-7.323	21.206	48.794	18.020	28.886	44.516	19.262	0.877
T33	-49.409	-45.728	-52.629	-55.716	-26.317	-28.579	-36.744	5.043	-0.364	-17.413	-26.680
span	20.766	26.503	19.848	7.511	31.531	52.147	21.435	33.511	46.937	22.874	14.194

Fig. 4. A front view photo of a test site inside KIGAM (left) field and a Wishart-H/$\bar{\alpha}$ classification result and the enlarged images extracted at 5 permanent scatterers, 2 man-made targets, and 4 trees positions and the polarimetric component values at the example positions listed in the below table.